Immunity, Volume *56*

Supplemental information

T cell-derived interleukin-22 drives the expression of CD155 by cancer cells to suppress NK cell function and promote metastasis

Daria Briukhovetska, Javier Suarez-Gosalvez, Cornelia Voigt, Anamarija Markota, Anastasios D. Giannou, Maryam Schübel, Jakob Jobst, Tao Zhang, Janina Dörr, Florian Märkl, Lina Majed, Philipp Jie Müller, Peter May, Adrian Gottschlich, Nicholas Tokarew, Jöran Lücke, Arman Oner, Melanie Schwerdtfeger, David Andreu-Sanz, Ruth Grünmeier, Matthias Seifert, Stefanos Michaelides, Michael Hristov, Lars M. König, Bruno Loureiro Cadilha, Oleg Mikhaylov, Hans-Joachim Anders, Simon Rothenfusser, Richard A. Flavell, Daniela Cerezo-Wallis, Cristina Tejedo, María S. Soengas, Tobias Bald, Samuel Huber, Stefan Endres, and Sebastian Kobold

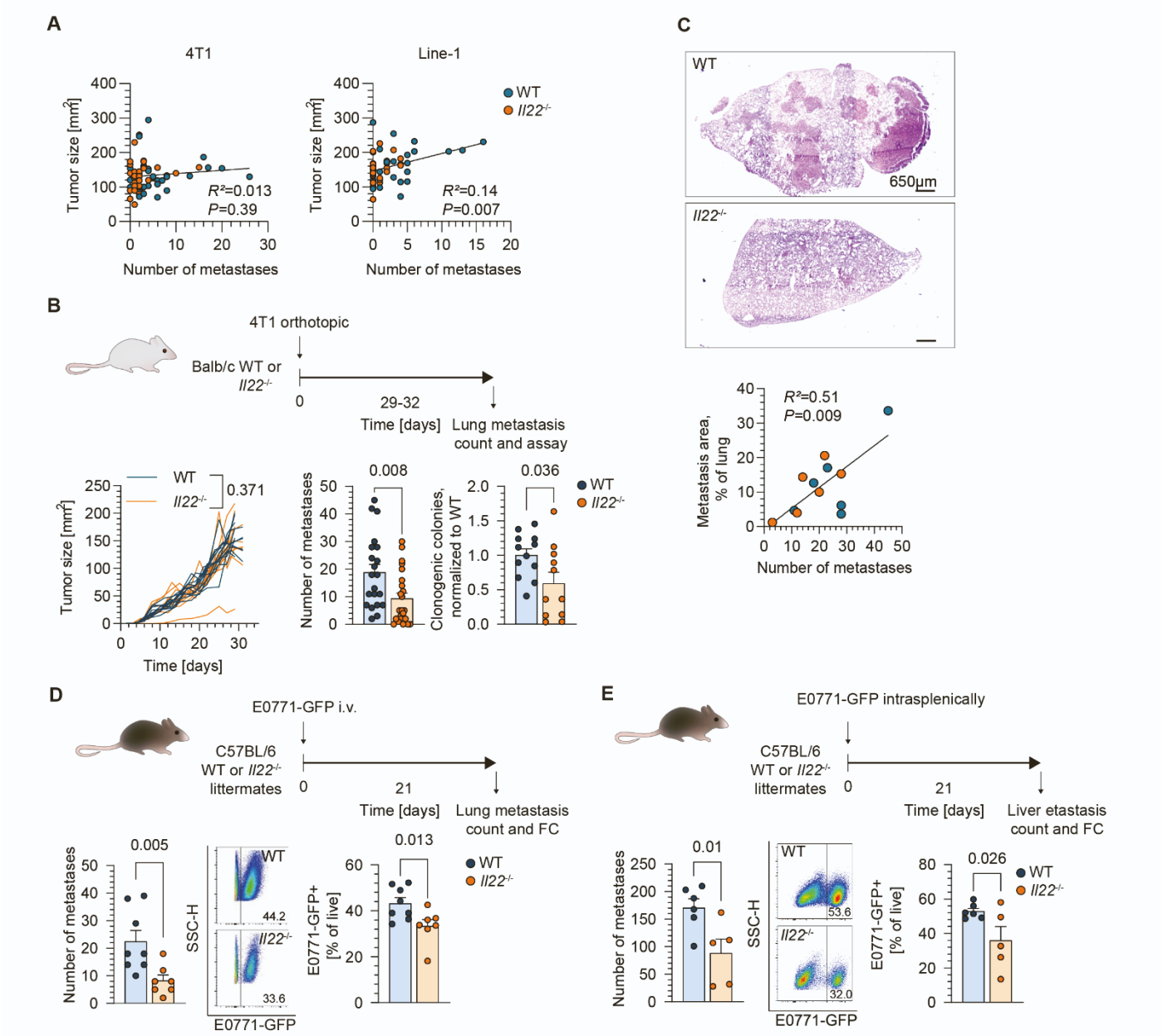

Figure S1, related to Fig. 1 IL-22 deficiency reduces the number of lung and liver metastases in syngeneic mouse models of lung and breast carcinoma. (**A**) Linear regression analysis of the correlation between the tumor size and the number of metastases from (Fig. 1). (**B**) Syngeneic 4T1 model of orthotopic mammary pad injection in WT and *Il22*$^{-/-}$ animals. Subcutaneous tumor growth, macroscopic metastases in the lungs, and colonies in clonogenic metastasis assay (n=20 for tumor growth and the number of metastases, n = 12 and 10 for clonogenic assay, data of three and two experiments pooled). (**C**) Representative microphotographs of HE-stained lung section with visible metastases. Linear regression analysis of macrometastasis vs metastatic area as a percent of the total area (n = 6). (**D**) Intravenous mouse model of E0771-GFP lung metastasis in WT and *Il22*$^{-/-}$ littermate mice. Numbers of metastases, representative flow cytometry plots, and frequency of E0771-GFP^{+}. The numbers are the frequency of the parent gate (n = 8 and 6). (**E**) Intrasplenic mouse model of E0771-GFP liver metastasis in WT and *Il22*$^{-/-}$ mice. Numbers of metastases in the liver, representative flow cytometry plots, and frequency of E0771-GFP^{+} cells. The numbers are the frequency of the parent gate. (n = 6 and 5). Data presented as means ± SEM, p-values < 0.05 were considered significant by the Mann-Whitney U test.

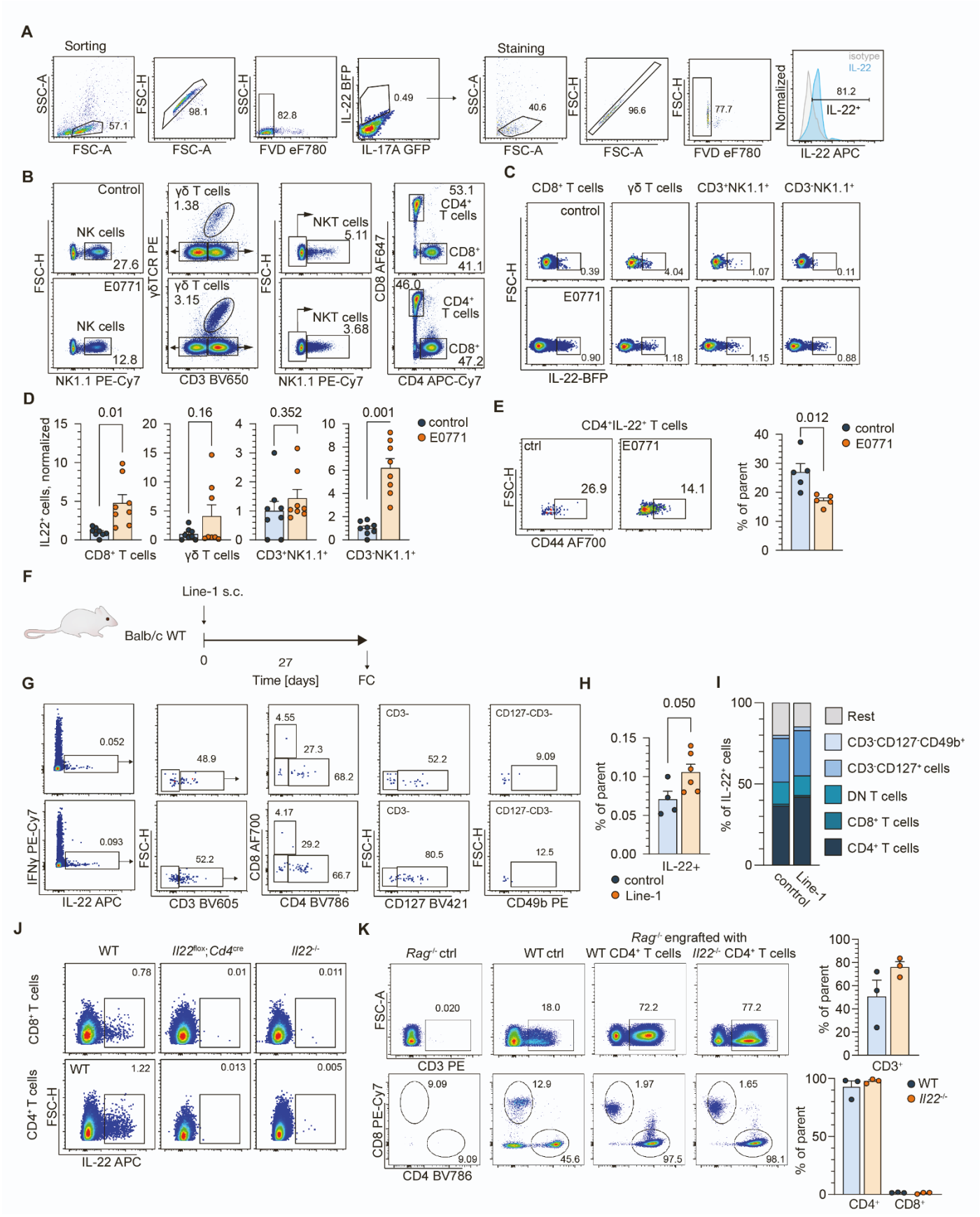

Figure S2, related to Fig. 2 T cells are the primary source of IL-22 in the lung of mice bearing subcutaneous tumors.

(**A**) Intracellular staining of FACS-sorted BFP+ cells from the lung of *Foxp3*^{mRFP}*Il17a*^{GFP}*Il22*^{sgBFP} mice. (**B**) Gating strategy to identify CD4$^+$, CD8$^+$ and double negative (DN) T cells, γδ T cells, CD3$^+$NK1.1$^+$, and CD3$^-$NK1.1$^+$ cells in the lungs of reporter mice and (**C**) IL-22 production in identified populations. Numbers represent the frequency of the parent

gate. (**D**) Percentage of IL-22^{+} cells normalized to control and reported per animal (n = 8). Data are presented as means ± SEM, and p-values <0.05 are considered significant as calculated by the Mann-Whitney U test. (**E**) CD44 expression by CD4^{+}IL-22^{+} T cells. (**F**) Subcutaneous model of Line-1 metastasis in WT and *Il22*$^{-/-}$ mice. (**G**) Gating strategy to identify CD4^{+}, CD8^{+} αβT cells, γδ T cells, CD3^{-}CD127^{+} ILCs, CD3^{-}CD49b^{+} NK cells in the lungs. Numbers represent the frequency of the parent gate. (**H**) Percentage of IL-22^{+} cells (n = 4 and 6). (**I**) Breakdown of IL-22^{+} cells by cell type as defined by the mean frequency of reported experiments. Data are presented as mean ± SEM, and a representative experiment of three is shown. P-values <0.05 are considered significant as calculated by the Mann-Whitney U test. (**J**) Intracellular IL-22 staining of Th17 polarized splenocytes from WT, *Il22*^{flox}*Cd4*^{cre,} and *Il22*$^{-/-}$ mice. (**K**) Engraftment of adoptively transferred MACS sorted WT and *Il22*$^{-/-}$ CD4+ T cells in the lungs of *Rag1*$^{-/-}$ mice 3 weeks post transfer. Representative dot plots, and frequency of total CD3^{+}, CD4$^{+,}$ and CD8^{+} cells are presented (n = 3).

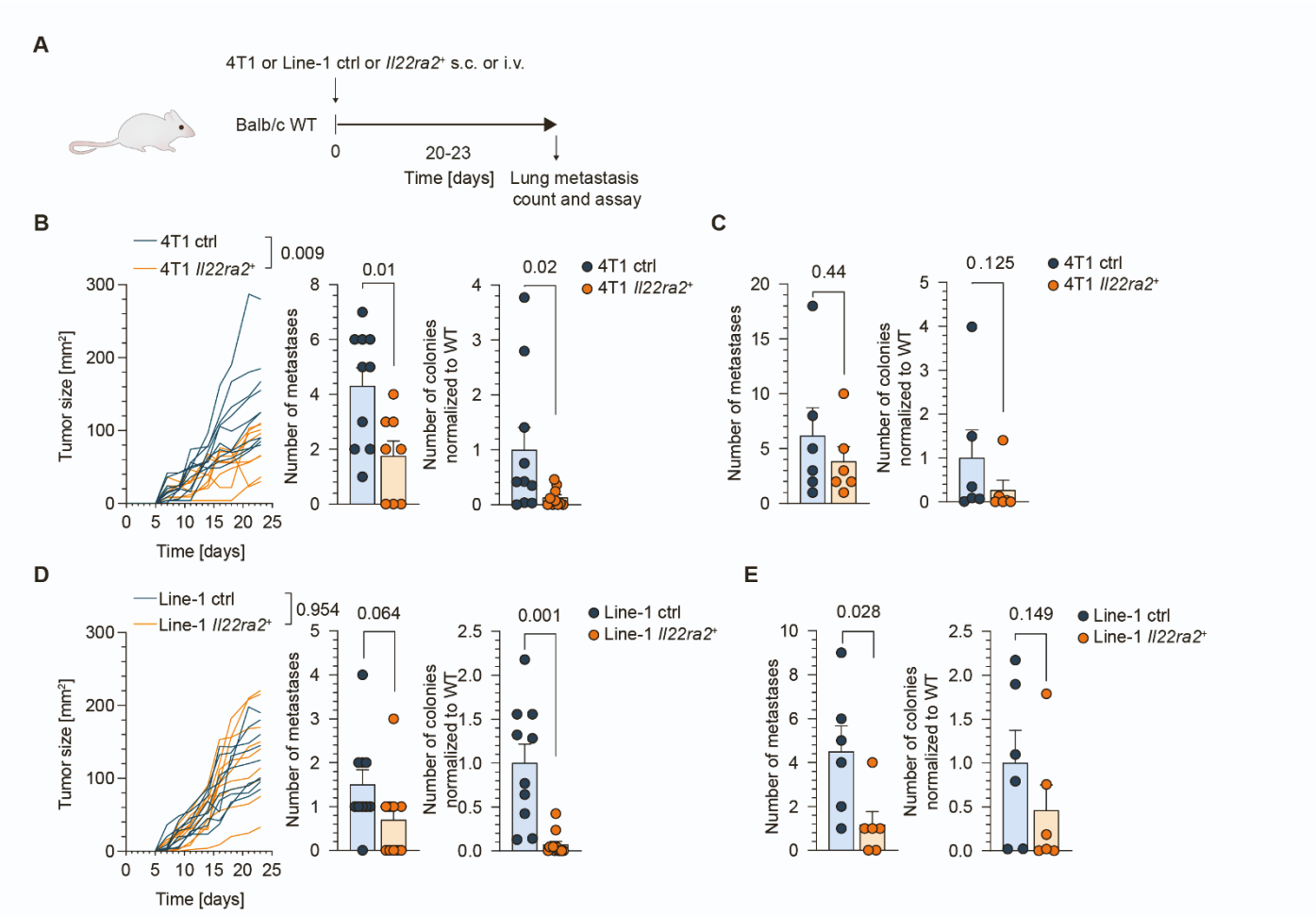

Figure S3, related to Fig. 3 IL-22BP reduces the number of lung metastases but does not affect tumor growth in subcutaneous and intravenous models of lung and breast carcinoma.

(**A**) Subcutaneous and intravenous mouse models of 4T1 and Line-1 *Il22ra2*$^{+}$ breast cancer metastasis. (**B**) Tumor size, the number of macroscopic metastases, and colonies in clonogenic metastasis assay in lungs from wild-type BALB/c mice injected s.c. with 4T1 control or 4T1 *Il22ra2*$^{+}$ cells as reported per animal (n = 10). Data from two independent experiments were pooled. (**C**) Numbers of macroscopic metastases and colonies in clonogenic metastasis assay injected i.v. with 4T1 control or *Il22ra2*$^{+}$ cells as reported per animal (n = 6). Data is from one experiment. (**D**) Tumor size, number of macroscopic metastases, and colonies in clonogenic metastasis assay in the lungs of mice injected s.c. with Line-1 control or *Il22ra2*$^{+}$ cells as reported per animal (n = 10). Data from two independent experiments were pooled. (**E**) Numbers of macroscopic metastases and colonies in clonogenic metastasis assay in the lungs of mice injected i.v. with Line-1 control or *Il22ra2*$^{+}$ cells as reported per animal (n = 6). Data are from one experiment and are represented as means ± SEM, p-values < 0.05 were considered significant by the mixed-effect two-way analysis for tumor growth and by the Mann-Whitney test for the number of metastases and colonies.

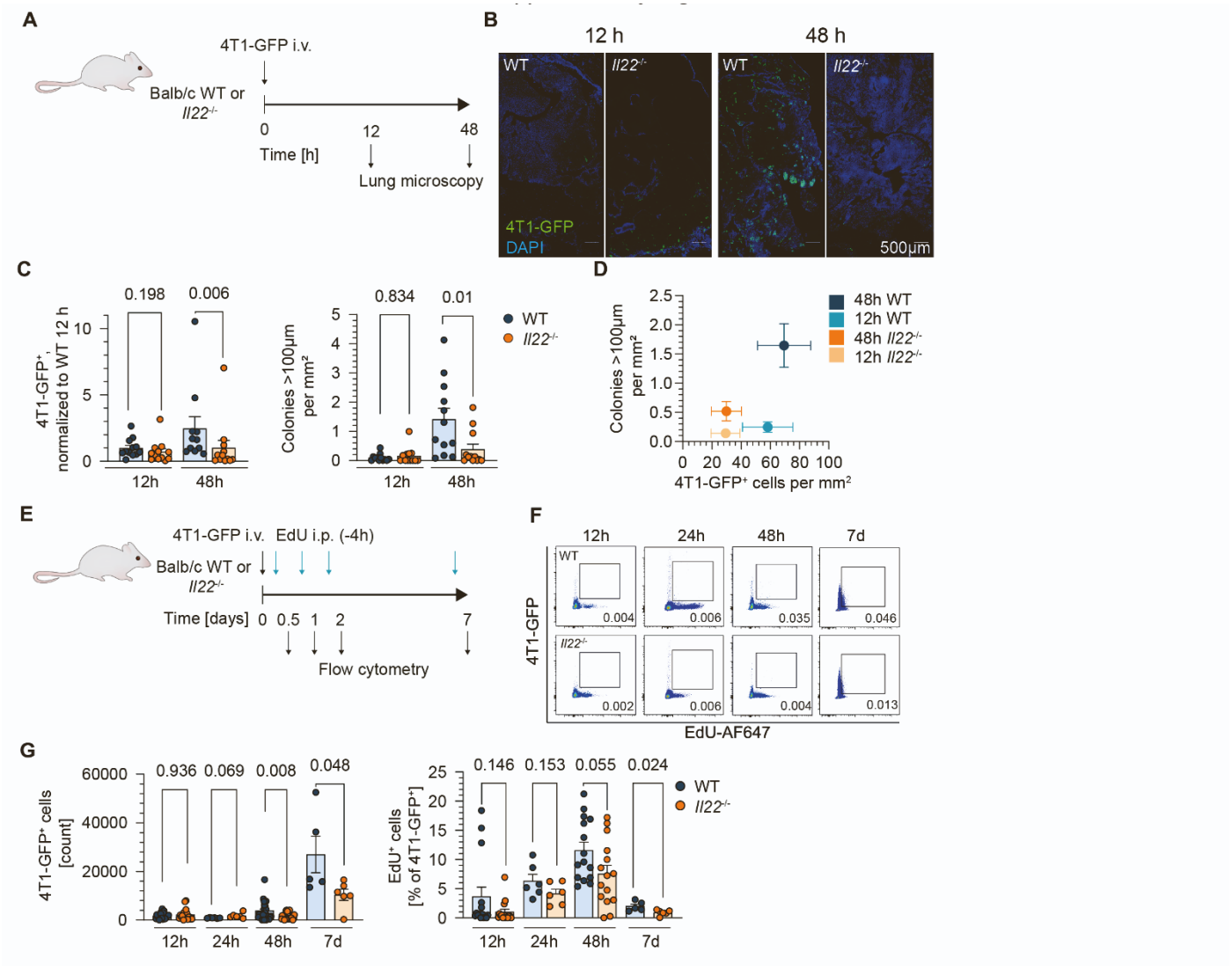

Figure S4, related to figure 3: IL-22 does not affect the seeding but the outgrowth of tumor cells during the early stages of engraftment.

(**A**) 4T1-GFP breast cancer model of seeding and outgrowth where WT and *Il22*$^{-/-}$ mice were sacrificed 12 or 48 hours after i.v. cancer cell injection. (**B**) Representative confocal images of the lungs. The GFP signal is depicted in green, and DAPI is in blue. (**C**) Numbers of individual 4T1-GFP cells and colonies larger than 100 µm per mm^2, normalized to the mean of WT control as reported for each mouse (n = 12). Data from three independent experiments were pooled. Data are presented as means ± SEM, and p-values < 0.05 are considered significant by the Mann-Whitney U test. (**D**) The correlation between the number of individual 4T1-GFP cells and the colonies larger than 100 µm in each condition is depicted by the mean of all samples ± SD. (**E**) Intravenous mouse model of 4T1-GFP breast cancer cell proliferation. Mice were co-injected with EdU four hours before preparation and sacrificed at 12-, 24-, 48-hour, and 7-day time points. (**F**) Representative contour plots of the lung cells. Numbers represent the frequency of the parent gate. (**G**) Total numbers of 4T1-GFP$^+$ cells in the lungs as reported per mouse (n = 19 and 25). Data from five independent experiments were pooled. Percentage of proliferating E0771-GFP$^+$ cells as reported per mouse (n = 15). Data from three independent experiments are pooled and are presented as means ± SEM, p-values < 0.05 are considered significant as calculated by the Mann-Whitney U test.

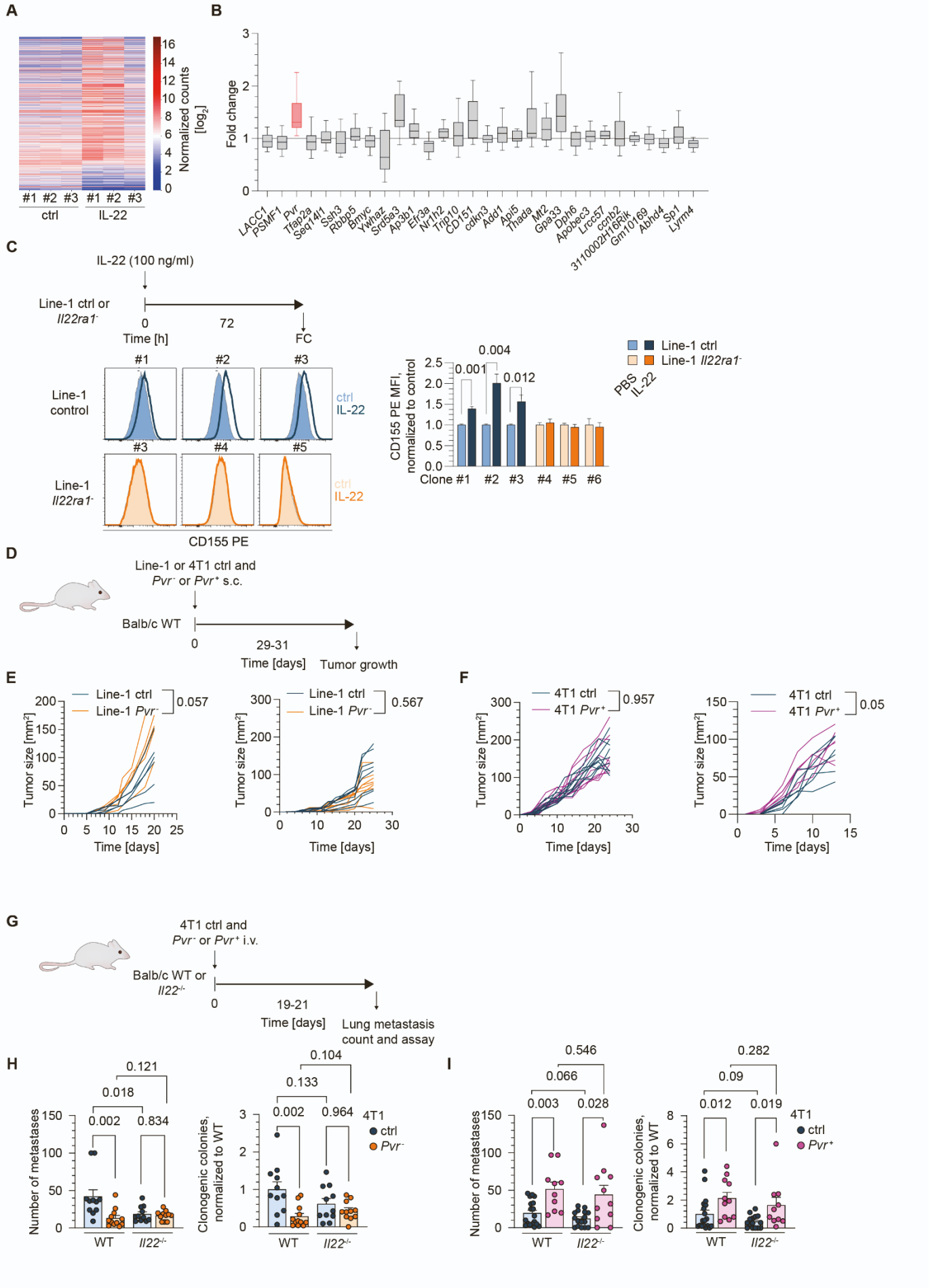
A
Normalized counts [log2]
16
14
12
10
8
6
4
2
0
#1 #2 #3 #1 #2 #3
ctrl
IL-22
B
Fold change
3
2
1
0
Lacc1
Psmf1
Pvr
Tfap2a
Seq14l1
Ssh3
Rbbp5
Bmyc
Ywhaz
Srd5a3
Ap3b1
Efr3a
Nr1h2
Trip10
CD151
cdkn3
Add1
Apl5
Thada
Mt2
Gpa33
Dph6
Apobec3
Lrcc57
ccnb2
3110002H16Rik
Gm10169
Abhd4
Sp1
Lyrm4
C
IL-22 (100 ng/ml)
Line-1 ctrl or
Il22ra1-
0
72
Time [h]
FC
#1
#2
#3
Line-1
control
ctrl
IL-22
#3
#4
#5
Line-1
Il22ra1-
ctrl
IL-22
CD155 PE
0.004
0.001
0.012
CD155 PE MFI,
normalized to control
2.5
2.0
1.5
1.0
0.5
0.0
Clone #1 #2 #3 #4 #5 #6
Line-1 ctrl
Line-1 Il22ra1-
PBS
IL-22
D
Line-1 or 4T1 ctrl and
Pvr- or Pvr+ s.c.
Balb/c WT
0
29-31
Time [days]
Tumor growth
E
Line-1 ctrl
Line-1 Pvr-
0.057
Tumor size [mm2]
200
150
100
50
0
0 5 10 15 20 25
Time [days]
Line-1 ctrl
Line-1 Pvr-
0.567
Tumor size [mm2]
300
200
100
0
0 10 20 30
Time [days]
F
4T1 ctrl
4T1 Pvr+
0.957
Tumor size [mm2]
300
200
100
0
0 10 20 30
Time [days]
4T1 ctrl
4T1 Pvr+
0.05
Tumor size [mm2]
150
100
50
0
0 5 10 15
Time [days]
G
4T1 ctrl and
Pvr- or Pvr+ i.v.
Balb/c WT or
Il22-/-
0
19-21
Time [days]
Lung metastasis
count and assay
H
0.121
0.018
0.002
0.834
Number of metastases
150
100
50
0
WT
Il22-/-
0.104
0.133
0.002
0.964
4T1
ctrl
Pvr-
Clonogenic colonies,
normalized to WT
3
2
1
0
WT
Il22-/-
I
0.546
0.066
0.003
0.028
Number of metastases
150
100
50
0
WT
Il22-/-
0.282
0.09
0.012
0.019
4T1
ctrl
Pvr+
Clonogenic colonies,
normalized to WT
8
6
4
2
0
WT
Il22-/-

Figure S5, related to Figure 5: (**A**) The heat plot reports the fold change of three individual control and IL-22 treated replicates in RNAseq. (**B**) Expression of the chosen differentially regulated genes as determined by RT-qPCR and presented as fold change over unstimulated control (n = 3). Data are presented as minimum, maximum, median, and quartiles. (**C**) CD155 expression in Line-1 *Il22ra1*$^{-}$ cells after stimulation with rmIL-22 (100 ng/ml) for 72 hours *in vitro.* Representative histograms of CD155 expression at 24, 48, and 72 hours and normalized MFI in three control and test clones. (**D**) Subcutaneous tumor growth of (**E**) Line-1 *Pvr*$^{-}$ (n = 6) and *Pvr*$^{+}$ (n = 8); 4T1 *Pvr*$^{-}$ (n = 9) and *Pvr*$^{+}$ (n = 6) cells in WT mice. (**G**) Intravenous mouse models of 4T1 *Pvr*$^{-}$ (**H**) and *Pvr*$^{+}$ (**I**) metastasis in WT or *Il22*$^{-/-}$ mice. Numbers of metastases and colonies in clonogenic metastasis assay as reported per animal (n = 14 and 17). Data from three independent experiments pooled, presented as means ± SEM, p-values < 0.05 were considered significant by the Mann-Whitney U test or mixed model analysis for tumor growth.

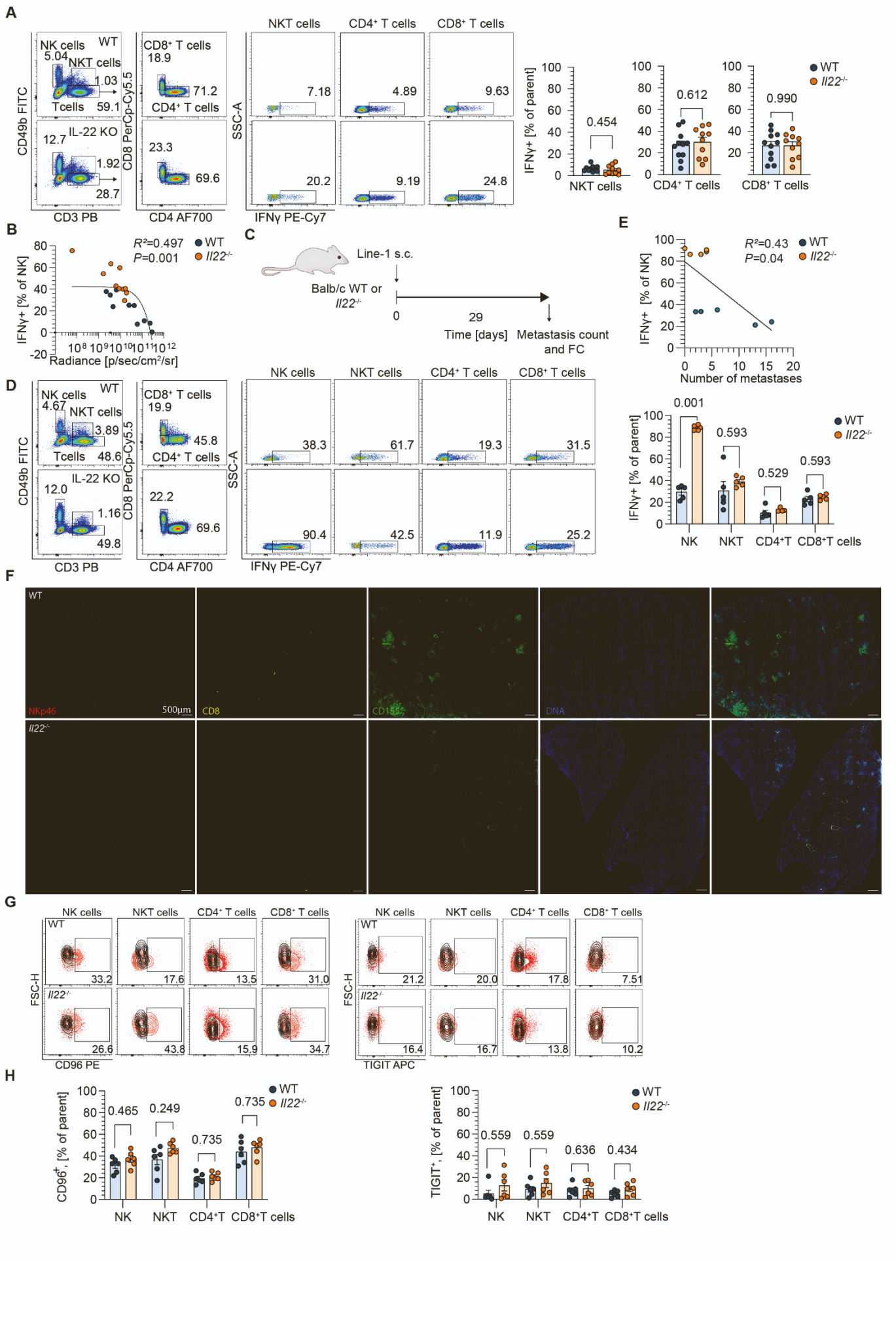
A
NK cells
WT
5.04
NKT cells
1.03
Tcells
59.1
IL-22 KO
12.7
1.92
28.7
CD49b FITC
CD3 PB
CD8⁺ T cells
18.9
71.2
CD4⁺ T cells
23.3
69.6
CD8 PerCp-Cy5.5
CD4 AF700
NKT cells
CD4⁺ T cells
CD8⁺ T cells
7.18
4.89
9.63
20.2
9.19
24.8
SSC-A
IFNγ PE-Cy7
IFNγ+ [% of parent]
0.454
0.612
0.990
NKT cells
CD4⁺ T cells
CD8⁺ T cells
WT
Il22-/-
B
R²=0.497
P=0.001
WT
Il22-/-
IFNγ+ [% of NK]
Radiance [p/sec/cm²/sr]
C
Line-1 s.c.
Balb/c WT or
Il22-/-
0
29
Time [days]
Metastasis count
and FC
E
R²=0.43
P=0.04
WT
Il22-/-
IFNγ+ [% of NK]
Number of metastases
D
NK cells
WT
4.67
NKT cells
3.89
Tcells
48.6
IL-22 KO
12.0
1.16
49.8
CD49b FITC
CD3 PB
CD8⁺ T cells
19.9
45.8
CD4⁺ T cells
22.2
69.6
CD8 PerCp-Cy5.5
CD4 AF700
NK cells
NKT cells
CD4⁺ T cells
CD8⁺ T cells
38.3
61.7
19.3
31.5
90.4
42.5
11.9
25.2
SSC-A
IFNγ PE-Cy7
0.001
0.593
0.529
0.593
WT
Il22-/-
IFNγ+ [% of parent]
NK
NKT
CD4+T
CD8+T cells
F
WT
NKp46
500µm
CD8
CD155
DNA
Il22-/-
G
NK cells
NKT cells
CD4⁺ T cells
CD8⁺ T cells
WT
33.2
17.6
13.5
31.0
Il22-/-
26.6
43.8
15.9
34.7
FSC-H
CD96 PE
NK cells
NKT cells
CD4⁺ T cells
CD8⁺ T cells
WT
21.2
20.0
17.8
7.51
Il22-/-
16.4
16.7
13.8
10.2
FSC-H
TIGIT APC
H
CD96⁺, [% of parent]
0.465
0.249
0.735
0.735
WT
Il22-/-
NK
NKT
CD4+T
CD8+T cells
TIGIT⁺, [% of parent]
0.559
0.559
0.636
0.434
WT
Il22-/-
NK
NKT
CD4+T
CD8+T cells

Figure S6, related to Figure 5: CD226, but not CD96 or TIGIT, is upregulated on NK cells of *Il22*$^{-/-}$ mice. (**A**) Representative dot plots and gating strategy of IFNγ producing CD8^{+} T cells, CD4^{+} T cells, and NKT cells in the lungs from (Fig. 5). Numbers represent the frequency of the parent gate. (**B**) Linear regression analysis of the correlation between the lung radiance and fraction of IFNγ^{+} NK cells in the lung from (Fig. 5). (**C**) Subcutaneous mouse model of Line-1 lung metastasis. (**D**) Gating strategy and (**E**) frequency of IFNγ production by CD8^{+} T cells, CD4^{+} T cells, NKT cells, and NK cells in the lung. Linear regression analysis of the correlation between the number of lung metastases and the IFNγ^{+} NK cells (n =5). (**F**) Entire fluorescent microscopy image overviews of the lungs of 4T1-injected WT and *Il22*$^{-/-}$ mice that were used for chip cytometry segmentation in Figure 5F. NKp46 FITC signal is depicted in red, CD8 AF555 in yellow, CD155 PE in green, and Hoechst DNA staining in blue. (**G**) Representative dot plots of CD96 and TIGIT staining on CD8^{+} T cells, CD4^{+} T cells, NKT cells, NK cells, and (**H**) frequency of CD96^{+} and TIGIT^{+} cells in the lungs. Numbers represent the frequency of the parent gate (n = 6, one representative experiment of 2). Isotype control is depicted in black. Data presented as means ± SEM, p-values < 0.05 were considered significant by the Mann-Whitney U test or multiple unpaired t-tests with Holm-Sidak correction.

A

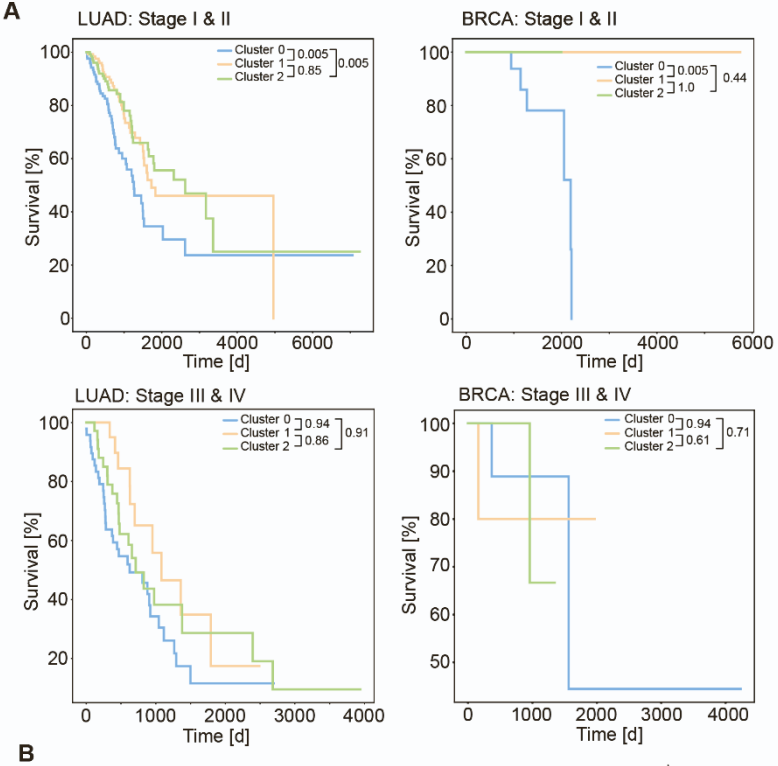

B

	coef	exp (coef)	se (coef)	coef upper 95%	coef lower 95%	exp(coef) upper 95%	exp(coef) lower 95%	z	p	-log2(p)
CD226	-0.24	0.79	0.13	0.01	-0.49	1.01	0.61	-1.88	0.06	4.05
CD96	0.09	1.09	0.14	0.37	-0.19	1.45	0.83	0.64	0.52	0.93
TIGIT	-0.02	0.98	0.15	0.27	-0.30	1.31	0.74	-0.13	0.90	0.15
IL22RA1	0.19	1.21	0.08	0.34	0.04	1.41	1.04	2.5	0.01	6.34
IL22RA2	-0.01	0.99	0.09	0.16	-0.19	1.17	0.83	-0.17	0.87	0.21
IL10RB	0.09	1.09	0.08	0.24	-0.06	1.28	0.94	1.14	0.25	1.97
PVR	0.25	1.28	0.07	0.39	0.11	1.48	1.11	3.39	<0.005	10.50

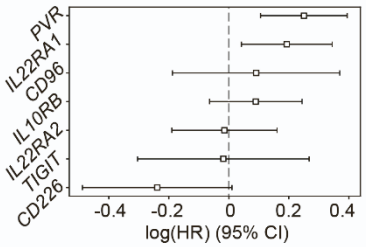

C

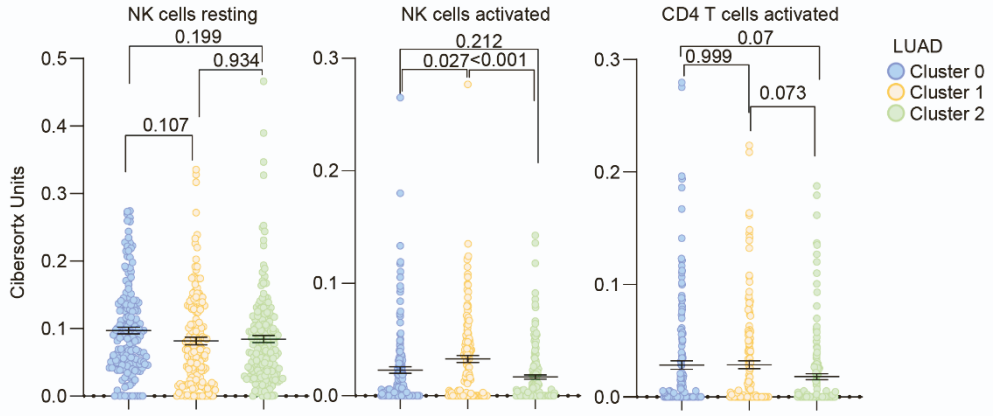

D

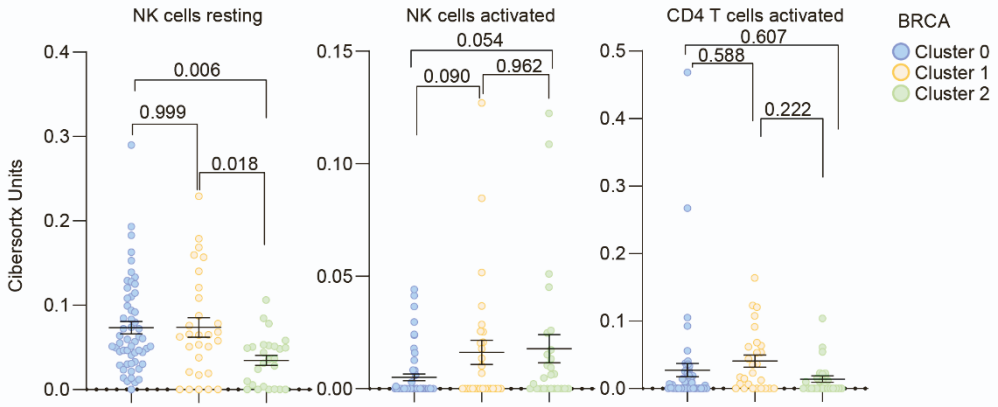

Figure S7, related to Figure 7: Regression and deconvolution analysis of TCGA datasets (**A**) Stage-specific survival of patients from LUAD and BRCA cohorts from Fig. 7. Log-rank (Mantel-Cox) test was used to compare curves. (**B**) Tabular results of Cox´s proportional hazards model, fit on TCGA LUAD cohort and plot of the log (Hazard Ratio) of regression. (**C**) Results of CIBERSORTx deconvolution on LUAD samples for resting and activated NK cells and activated $CD4^+$ memory T cells in absolute units, showing different immune cell infiltrates for the IL-22 PVR Clusters. (**D**) CIBERSORTx results in BRCA samples for the previously mentioned immune-cell subtypes. P-values <0.05 were considered significant by Tukey´s multiple comparisons test (for CIBERSORTx results) or Cox´s proportional hazards models. Lines and whiskers indicate mean ± SEM for CIBERSORTx results, and squares and whiskers indicate $\log_2$(HR) and 95% confidence interval for Cox´s proportional hazards model.

Table S1, related to STAR methods: Oligonucleotides used in this study.

Oligo Name	Purpose	Source	Sequence	Probe (Universal Probe library from Sigma)	Catalog number
oIMR1084 Fw	Genotyping CMV-cre mice	Jackson Laboratory	GCGGTCTGGCAGTAAAAACTATC	N/A	N/A
oIMR1085 Rw	Genotyping CMV-cre mice	Jackson Laboratory	GTGAAACAGCATTGCTGTCACTT	N/A	N/A
CD4-cre Fw	Genotyping CD4-cre mice	IMI, Munich	CCCAACCAACAAGAGCTC	N/A	N/A
CD4-cre Rw	Genotyping CD4-cre mice	IMI, Munich	CCCAGAAATGCCAGATTACG	N/A	N/A
DNA460-40 Fw	Genotyping 12955-IL22TM1.1LEX/ Mmuccl	Lexicon genetics (UNQ3099)	CTCAGACCTCTACAGACAATCATC	N/A	N/A
DNA460-41 Rw	Genotyping 12955-IL22TM1.1LEX/ Mmuccl	Lexicon genetics (UNQ3099)	GATACAGGTGCAGCTAAGCGAG	N/A	N/A
sgRNA *Il22ra1*	CRISPR-Cas9 gene edition	CHOPCHOP v.3	CTACTGACCATCCTGACGGT	N/A	N/A
sgRNA *Pvr*	CRISPR-Cas9 gene edition	CHOPCHOP v.3	GCTTCTAATCTCCACCGTAG	N/A	N/A
Il22ra2 Fw	PCR	ProbeFinder 2.53	ACAACAGCATCTACTTTGTGCAG	N/A	N/A
Il22ra2 Rw	PCR	ProbeFinder 2.53	CCCCCAGCAGTCAACTTTAT	N/A	N/A
l22ra2 clone Fw	Cloning	This paper	ATTACTCGAGGCCACCATGATGC CTAAG	N/A	N/A
l22ra2 clone Rw	Cloning	This paper	TAATGAATTCTCATGGAATGTGC ACACATCTCTCC	N/A	N/A
CD155-Frag1.FOR	Cloning	This paper	TACAGGCGGCCGCGCCACCATGG CTCAACTCGCCC	N/A	N/A
CD155-Frag2.FOR	Cloning	This paper	CAGCACAAGGGTGAAACAGACTT TGAATTTTGACCTTCT	N/A	N/A
CD155-Frag3.FOR	Cloning	This paper	CCAGGCCCGATGCCAGAGCCAGC G	N/A	N/A
CD155-Frag1.REV	Cloning	This paper	TCTGTTTCACCCTTGTGCTGTTTG GCTC	N/A	N/A
CD155-Frag2.REV	Cloning	This paper	GGCATCGGGCCTGGGTTGG	N/A	N/A
CD155-Frag3.REV	Cloning	This paper	TGCTCGAATTCTTACTTGTACAGC TCGTCCATG	N/A	N/A

3110002H16Rik Fw	RT-PCR	ProbeFinder 2.53	CATTATCAGTGCAAGCCAAGG	#41	Cat# 4688007001
3110002H16Rik Rw	RT-PCR	ProbeFinder 2.53	CCTTTATCTGGCAAGAGATTCAC	#41	Cat# 4688007001
Add1 Fw	RT-PCR	ProbeFinder 2.53	GGGTGATGACGCTTCTGAG	#38	Cat# 4687957001
Add1 Rw	RT-PCR	ProbeFinder 2.53	TGTCCATCCTCTTTAGTCCACTT	#38	Cat# 4687957001
Ap3b1 Fw	RT-PCR	ProbeFinder 2.53	GAAACACCAAGCCGTTGC	#15	Cat# 4685130001
Ap3b1 Rw	RT-PCR	ProbeFinder 2.53	AGCTGAGCGACAGCCATAAC	#15	Cat# 4685130001
Api5 Fw	RT-PCR	ProbeFinder 2.53	CCTCAGCACCCTGACCAC	#97	Cat# 4692136001
Api5 Rw	RT-PCR	ProbeFinder 2.53	AACTCATCTCTGCCAACAACTTTA	#97	Cat# 4692136001
Apobec3 Fw	RT-PCR	ProbeFinder 2.53	CTGCTTACAAATTTTAGATACCAGGA	#11	Cat# 4685105001
Apobec3 Rw	RT-PCR	ProbeFinder 2.53	ACAGATATTTGACAGAGTGGATGAA	#11	Cat# 4685105001
Bmyc Fw	RT-PCR	ProbeFinder 2.53	CCAAGCTGGTCTCCAAGC	#64	Cat# 4688627001
Bmyc Rw	RT-PCR	ProbeFinder 2.53	CGTAGCAGGCTCCACGTC	#64	Cat# 4688627001
ccnb2 Fw	RT-PCR	ProbeFinder 2.53	CAACCGTACCAAGTTCATCG	#84	Cat# 4689062001
ccnb2 Rw	RT-PCR	ProbeFinder 2.53	GAGGGATCGTGCTGATCTTC	#84	Cat# 4689062001
CD151 Fw	RT-PCR	ProbeFinder 2.53	CGCTCACTGGTGTTCCTAGTC	#16	Cat# 4685148001
CD151 Rw	RT-PCR	ProbeFinder 2.53	CTCAGAGCCACCAGATCTCA	#16	Cat# 4685148001
cdkn3 Fw	RT-PCR	ProbeFinder 2.53	GATGAAGAACAGACTCCAATTCAA	#48	Cat# 4688074001
cdkn3 Rw	RT-PCR	ProbeFinder 2.53	AACCTGGAAGAGCACATAAACC	#48	Cat# 4688074001
Dph6 Fw	RT-PCR	ProbeFinder 2.53	CAACGTGGACGAGTAGAAAATG	#19	Cat# 4686918001
Dph6 Rw	RT-PCR	ProbeFinder 2.53	TCTCTCGGAGCAAATCTTCC	#19	Cat# 4686918001
Efr3a Fw	RT-PCR	ProbeFinder 2.53	GCTTCATGATAGACTTGCTCAAATA	#52	Cat# 4688589001
Efr3a Rw	RT-PCR	ProbeFinder 2.53	GTAACGGTCAATGTTCCAGATG	#52	Cat# 4688589001
Gm10169 Fw	RT-PCR:	ProbeFinder 2.53	GCCAGAGGGGTTTCTGTCT	#3	Cat# 4684982001
Gm10169 Rw	RT-PCR	ProbeFinder 2.53	TTCGTGCCGCTAAAAGTCAT	#3	Cat# 4684982001
Gpa33 Fw	RT-PCR	ProbeFinder 2.53	GTCCGCCTCTTGGTCCTT	#89	Cat# 4689135001
Gpa33 Rw	RT-PCR	ProbeFinder 2.53	GTTGTTCCCGATCACCATCT	#89	Cat# 4689135001
LACC1 Fw	RT-PCR	ProbeFinder 2.53	TTGGCTTCATATCCCTTAGAGAA	#19	Cat# 4686918001
LACC1 Rw	RT-PCR	ProbeFinder 2.53	GGAAGGATGCAGGAAACATC	#19	Cat# 4686918001
Lrcc57 Fw	RT-PCR	ProbeFinder 2.53	AAACTTCGAGAACTAGAGGGTTATGA	#76	Cat# 4688988001
Lrcc57 Rw	RT-PCR	ProbeFinder 2.53	GATCCTGGAGAATATCATGCAA	#76	Cat# 4688988001
Lyrm4 Fw	RT-PCR	ProbeFinder 2.53	GCATTTCAGCGCCTACAATTA	#2	Cat# 4685091001
Lyrm4 Rw	RT-PCR	ProbeFinder 2.53	TCACCAGGGCTTGAATTTCT	#2	Cat# 4685091001
Mt2 Fw	RT-PCR	ProbeFinder 2.53	CATGGACCCCAACTGCTC	#4	Cat# 4685008001
Mt2 Rw	RT-PCR	ProbeFinder 2.53	AGCAGGAGCAGCAGCTTT	#4	Cat# 4685008001
Nr1h2 Fw	RT-PCR	ProbeFinder 2.53	AGCTCTGCCTACATCGTGGT	#106	Cat# 4692241001
Nr1h2 Rw	RT-PCR	ProbeFinder 2.53	AAGCCTTGTCTCCGCACA	#106	Cat# 4692241001
PSMF1 Fw	RT-PCR	ProbeFinder 2.53	CTGTGGAGAACGGCATGAT	#62	Cat# 4688937001
PSMF1 Rw	RT-PCR	ProbeFinder 2.53	CATCTAAGTTCAGGGTCAAGTCTG	#62	Cat# 4688937001
PVR Fw	RT-PCR	ProbeFinder 2.53	TGACCCTTTCCCAACCCTAT	#106	Cat# 4692241001
PVR Rw	RT-PCR	ProbeFinder 2.53	GAGGCCAACATACCAGTTGC	#106	Cat# 4692241001
Rbbp5 Fw	RT-PCR	ProbeFinder 2.53	GTAAAGTGCAGGCGGAACTC	#18	Cat# 4686900001
Rbbp5 Rw	RT-PCR	ProbeFinder 2.53	TTCACAGCAGTTCTGAGATGG	#18	Cat# 4686900001
Sec14l1 Fw	RT-PCR	ProbeFinder 2.53	CGGGTGTATAAACATCCCTTTG	#46	Cat# 4688058001
Sec14l1 Rw	RT-PCR	ProbeFinder 2.53	GGACATGTAGGAAACCTCCTCTC	#46	Cat# 4688058001
Sp1 Fw	RT-PCR	ProbeFinder 2.53	GCCCCTATTGCAAAGACAGT	#103	Cat# 4692209001

Sp1 Rw	RT-PCR	ProbeFinder 2.53	GCATCCTTGGATGTGACAAA	#103	Cat# 4692209001
Srd5a3 Fw	RT-PCR	ProbeFinder 2.53	TTCGATGTCCCCAAGAGGTA	#106	Cat# 4692241001
Srd5a3 Rw	RT-PCR	ProbeFinder 2.53	TCCCAGGAACAACGACTGA	#106	Cat# 4692241001
Ssh3 Fw	RT-PCR	ProbeFinder 2.53	TCATGGTGGAGCTGCTGA	#26	Cat# 4687574001
Ssh3 Rw	RT-PCR	ProbeFinder 2.53	ACCAGCAGGTAGCGAAGTCT	#26	Cat# 4687574001
Tfap2a Fw	RT-PCR	ProbeFinder 2.53	CAAGTACGAAGACTGCGAGGA	#104	Cat# 4692217001
Tfap2a Rw	RT-PCR	ProbeFinder 2.53	GCTGGTGTAGGGAGATTGACC	#104	Cat# 4692217001
Thada Fw	RT-PCR	ProbeFinder 2.53	TCAGGCATCTACTGATACTGGAAC	#82	Cat# 4689151001
Thada Rw	RT-PCR	ProbeFinder 2.53	GAGACACGCCATCAAAGCTC	#82	Cat# 4689151001
Trip10 Fw	RT-PCR	ProbeFinder 2.53	TTTCGGGAAAAAGAACAAGC	#79	Cat# 4689011001
Trip10 Rw	RT-PCR	ProbeFinder 2.53	GACAGTGTGGAGGGTAGGTGA	#79	Cat# 4689011001
Ywhaz Fw	RT-PCR	ProbeFinder 2.53	TAAAAGGTCTAAGGCCGCTTC	#71	Cat# 4688945001
Ywhaz Rw	RT-PCR	ProbeFinder 2.53	CACCACACGCACGATGAC	#71	Cat# 4688945001